IOP Publishing and International Atomic Energy Agency Nuclear Fusion
Nucl. Fusion **52** (2012) 094003 (9pp) doi:10.1088/0029-5515/52/9/094003

# Simulation and theory of spontaneous TAE frequency sweeping

**Ge Wang and H.L. Berk**

Institute for Fusion Studies, The University of Texas at Austin, Austin, TX 78712, USA

E-mail: wange@ph.utexas.edu

Received 30 January 2012, accepted for publication 3 July 2012
Published 3 September 2012
Online at stacks.iop.org/NF/52/094003

**Abstract**
A simulation model, based on the linear tip model of Rosenbluth, Berk and Van Dam (RBV), is developed to study frequency sweeping of toroidal Alfvén eigenmodes (TAEs). The time response of the background wave in the RBV model is given by a Volterra integral equation. This model captures the properties of TAE waves both in the gap and in the continuum. The simulation shows that phase space structures form spontaneously at frequencies close to the linearly predicted frequency, due to resonant particle–wave interactions and background dissipation. The frequency sweeping signals are found to chirp towards the upper and lower continua. However, the chirping signals penetrate only the lower continuum, whereupon the frequency chirps and mode amplitude increases in synchronism to produce an explosive solution. An adiabatic theory describing the evolution of a chirping signal is developed which replicates the chirping dynamics of the simulation in the lower continuum. This theory predicts that a decaying chirping signal will terminate at the upper continuum though in the numerical simulation the hole disintegrates before the upper continuum is reached.

(Some figures may appear in colour only in the online journal)

## 1. Introduction

The toroidal Alfvén eigenmode (TAE) is a shear Alfvén-like mode in toroidal devices that lies within a frequency gap surrounded by the MHD continuum [1]. These waves can be spontaneously excited due to the resonant particle–wave interaction if nonlinear free energy can be released by the resonant particles. If dissipation in the background plasma is present, and if the plasma is at low enough collisionality, TAE waves are likely to form resonant phase space structures in the frequency gap which may then chirp into the continuum. The initial evolution of the phase space structure is quite similar to the most simplified model described by the electrostatic bump-on-tail instability [2–4]. However, once the frequency shift becomes comparable to the frequency shift between the linearly predicted frequency and the continuum frequency, the standard theory is inapplicable. Here we will exhibit a new model for describing phase space chirp of TAE modes that has the possibility of chirping into the surrounding continuum. The governing equations for this model are based on the linear tip model of Rosenbluth, Berk and Van Dam (RBV), which describes the TAE excitation in a large aspect ratio, circular tokamak at low beta. To simplify the calculation we deal with a case where the TAE excitation is primarily from a single couplet which consists of a wave with a poloidal structure consisting dominantly of the $m$th and $(m+1)$th poloidal harmonic localized near the region where $q(r_m) = (m+1/2)/n \equiv q_m$. We assume that the interaction with neighbouring couplets can be ignored which is best satisfied at low shear.

The original theory for the tip model was derived in frequency space. Using the Fourier transform, the frequency form can be converted to a convolution integral with a temporal kernel producing a non-local time response for the wave. The governing theory for the time representation of the RBV tip model has been described in a recent paper [5]. In this paper we show how to develop an adiabatic theory for the RBV-resonant particles and waves. During adiabatic evolution of a TAE wave amplitude and its chirping rate, parameters need to evolve slowly in one bounce period. Then the dynamics of energetic particles in the trapping region of a hole or clump can be described with action-angle variables, where the canonical action variable $J$ is an adiabatic invariant. The distribution function of energetic particles is given by $f(J)$ which remains constant in time, except for the change of the distribution function at the separatrix where particles are entrapped by or lost from the trapping region. This theory leads to results that for the most part closely replicate the results of the Vlasov simulations.

This paper is organized as follows: a brief introduction to the RBV-TAE model and the Vlasov simulation is given

 

in section 2. The adiabatic theory is discussed in section 3. We compare and interpret the results between the Vlasov simulation and adiabatic calculation in section 4. Section 5 contains final concluding comments. An appendix is included which analyses the adiabatic chirping theory for a hole near the upper continuum.

## 2. The Vlasov simulation

In this section we largely present previously reported results from a dynamic simulation of a TAE mode. A model is based on the linear tip theory of RBV for the TAE wave [6], which is valid for a small inverse aspect ratio and low beta tokamak. The RBV theory leads to a Volterra integral equation in the time domain for the evolution of the wave. To this equation we add, using a simplified model, an interaction term of the wave and energetic particles. The particles are taken to satisfy a one dimensional Vlasov equation given in terms of action-angle variables. The dynamics of the resonant particles is then the same as the dynamics in the bump-on-tail problem. Integrating in phase space we then calculate the particle–wave interaction term. This term is formally a source for the linear wave equation for TAE excitations. In the time domain the TAE excitation has been shown to be described by a Volterra equation [5]. Without dissipation, the Volterra equation coupled to the energetic particle interaction term produces a linear instability with a growth rate $\gamma_{\rm L}$. We then add to the equation two extrinsic dissipation mechanisms which will be described below. The dissipation produces a damping rate $\gamma_{\rm d}$. We select enough dissipation to create an initial system with energetic particles close to marginal stability, with a growth rate $\gamma = \gamma_{\rm L} - \gamma_{\rm d} \ll \gamma_{\rm L}$. In the simulation we see an initial formation of the phase space structures with their subsequent chirps. Initially the characteristic of the chirp is similar to what has been described for the bump-on-tail problem [3]. However, in the subsequent evolution, new chirping properties appear as the excited wave chirps towards the continuum and then often into the continuum.

The wave equation, including the interaction with the resonant particles, takes the form [5]

$$(\Delta_m - i)A(t) - \int_0^t (J_0(t-\tau) - \mathrm{i}J_1(t-\tau))\mathrm{e}^{-\gamma_{\rm d}'(t-\tau)}A(\tau)\,\mathrm{d}\tau = -\frac{\mathrm{i}\eta}{\pi}\int_{-\infty}^{\infty} f(p,\theta,t)\mathrm{e}^{-\mathrm{i}\theta}\,\mathrm{d}p\,\mathrm{d}\theta, \quad (1)$$

where the left-hand side (LHS) is the linear response due to the electromagnetic field and the background plasma, and the right-hand side (RHS) describes the interaction of the resonant particle currents with the linear wave. The factor $\eta$ is proportional to the linear growth rate and later will be explicitly defined. The real component of the parameter $\Delta_m$ ($\Delta_r = \Re\Delta_m$) is obtained from the ideal MHD contribution of the predominant poloidal $m$th and $(m+1)$th components of an Alfvénic mode outside the gap region, while the frequency-dependent items represent the ideal MHD contribution in the vicinity of the gap. Parameters are scaled so that the band frequency in the gap lies between $-1 \leqslant \omega \leqslant 1$. With this frequency normalization the linear TAE frequency is given by $\omega_0 = (\Delta_r^2 - 1)/(\Delta_r^2 + 1)$. In the ideal MHD theory where there is no dissipation, the eigenmode frequency is always in the gap and never in the continuum. In addition to produce damping in the gap region, extrinsic dissipation is added to our model with the parameters chosen to produce a given damping rate $\gamma_{\rm d}$. Two dissipative parameters are chosen to capture the dissipation due to non-ideal MHD effects. The parameter $\gamma_{\rm d}'$ mocks up damping arising from non-MHD effects at spatial positions near the tip region, while the imaginary component of the parameter $\Delta_m$ ($\Delta_{\rm i} = \Im\Delta_m$) is used to capture dissipation arising from non-MHD effects outside the TAE interaction region. In general we can treat a combination of the two parameters, using a single parameter $\beta$, with $0 \leqslant \beta \leqslant 1$ where the two dissipative parameters are given by $\gamma_{\rm d}' = \beta\gamma_{\rm d}$ and $\Delta_{\rm i} = (1-\beta)\Delta_{\rm i0}$, with $\Delta_{\rm i0} = -\lambda\gamma_{\rm d}$ where $\lambda = (\Delta_r^2+1)^2/(4\Delta_r)$. Note that for any $\beta$ the sum of these two terms gives the same damping rate $\gamma_{\rm d}$ when $\gamma_{\rm d} \ll 1$. To see if there is any sensitivity to the nonlinear results with the choice of dissipation models, the simulations have primarily been performed for the two extremes: cases (I) $\gamma_{\rm d}' = \gamma_{\rm d}$, and $\Delta_{\rm i} = 0$ and case (II) $\gamma_{\rm d}' = 0$ and $\Delta_{\rm i} = \Delta_{\rm i0}$ ($\Delta_{\rm i0}$ is finite and negative). Both models produce nearly the same response in the linear phase and the early chirping response where the theory of [3] applies. However, with increasing frequency shift, the choice of the dissipation model changes the quantitative dynamical evolution though not the qualitative conclusion.

With the RBV tip theory the $m$th and $(m+1)$th poloidal harmonics are intrinsically linked together when the frequencies are close to and within the gap. As the chirping frequency moves away from the gap frequency, the two mode components decouple. For example, if the safety factor increases with minor radius, then for downward chirp of a clump into the continuum, the mode structure becomes more dependent on the $m$th component as the $(m+1)$th component reduces in amplitude. Similarly, the $(m+1)$th poloidal harmonic will eventually dominate as a hole chirps into the upper continuum. The results that emerge from the tip model are justified as long as the inverse aspect ratio is small, $\omega(t) - \omega_A \ll \omega_A$ ($\omega_A$ is the central frequency in the gap) and the MHD excitations at the nearest neighbouring tip positions (e.g. at $r \sim r_{m+1}$, where $q(r_{m+1}) = (m+3/2)/n$) is negligible.

The RHS of equation (1) is the response of the resonant particle region, which depends on the dynamical particle distribution $f$. The kinetic Vlasov equation is used to describe the dynamics of collisionless particles with a distribution function characterized by a single pair of action-angle variables $(p,\theta)$ of the unperturbed orbits. The Vlasov equation is

$$\frac{\partial f}{\partial t} + p\frac{\partial f}{\partial \theta} - \Re(A(t)\mathrm{e}^{\mathrm{i}\theta})\frac{\partial f}{\partial p} = 0. \quad (2)$$

Note that collisions, which are of considerable importance under many conditions, e.g. [3, 4, 7], have been neglected as a simplifying ansatz in this study.

The algorithm used to solve the Vlasov equation has been changed from the original work of Petviashvili [8]. In Petviashvili's numerical scheme, the Vlasov equation is solved in the Fourier space $(s,n)$ of the action-angle variables $(p,\theta)$. The integration was based on an iterative scheme where the implicit part of the inversion arises from the free streaming terms while the interaction term is treated as a source term whose form is updated during the iteration. The iteration comes at a cost of computational time that prevents efficient

code parallelization. Our present Vlasov solver avoids the iterative process and solves the Fourier transformed Vlasov equation along each individual free streaming characteristic line as a tri-diagonal matrix equation. The resulting code is then suitable for parallelization along a set of characteristic lines. In this method the computational time is reduced by an order of magnitude.

The distribution function is not usually a smooth function around the separatrix region of a structure. As a result, a Gibbs phenomenon is found when the distribution function in the Fourier space is converted to the physical space. Gibbs' ripples appear inside the resonant structure. Fortunately, the source term $-(i\eta/\pi)\int_{-\infty}^{\infty} f(p,\theta,t)e^{-i\theta}\,dp\,d\theta$ appearing in the wave equation still maintains accuracy for a long time even with the Gibbs ripple phenomenon present as has been investigated in [9]. Therefore, we apparently obtain the correct wave response, though the Gibbs phenomenon becomes more pronounced as time evolves especially when viewing the distribution function in the $(p,\theta)$ phase space. An additional approximation is to set a non-reflection boundary condition at the boundary positions of $s = \pm s_{\max}$ to avoid largely false signals from being reflected from these boundaries. However, even this boundary condition can lead to trouble late in time when an aliasing problem sometimes develops. With an alternative procedure that smoothly filters the large $s$ data, we have largely removed this aliasing problem.

The velocity frame of the phase space structure is tracked in our numerical scheme. This tracking allows a shift of the computation frame from the 'lab' frame to a wave frame. The tracking region is localized to lie within $-\pi \leqslant \theta \leqslant \pi$ and $p_- \leqslant p \leqslant p_+$, where $p_-$ and $p_+$ are defined as the lower and upper bounds of a velocity window transfering to the wave frame. For a clump/hole that is in the tracking region, the velocity of the wave frame $v_f$ is determined by demanding that the overall relative acceleration of the region vanishes.

$$dv_f/dt = -\int_{-\pi}^{\pi}\int_{p_-}^{p_+} f(p,\theta,t)\Re(A(t)e^{i\theta})\,dp\,d\theta \Big/ \int_{-\pi}^{\pi}\int_{p_-}^{p_+} f(p,\theta,t)\,dp\,d\theta = 0. \quad (3)$$

Note that in the above equation we are using coordinate information only within the tracking region.

In this computational frame the chirping signal of interest only oscillates at a low frequency. Then in accord with the Nyquist–Shannon sampling theorem [10], a moderately large time step $\Delta t$ can be taken and the targeted phase space structure can evolve and be accurately described even when the phase space structure of interest produces a large frequency shift in the laboratory frame. The method of tracking given in equation (3) was developed after we found an unacceptable tracking error emerging when we attempted to use a band-pass filter to extract the frame of the wave by tracking the peak intensity of the wave spectrum. The spectral method was particularly deficient during the early stages of the evolution, when the frequencies from different structures are close together. Then the mixing of signals from adjacent structures produces a great deal of noise which leads to difficulty in obtaining an early comparison of the simulation results with that of adiabatic theory. This problem is substantially alleviated when the frame of the wave is determined at every time step by equation (3).

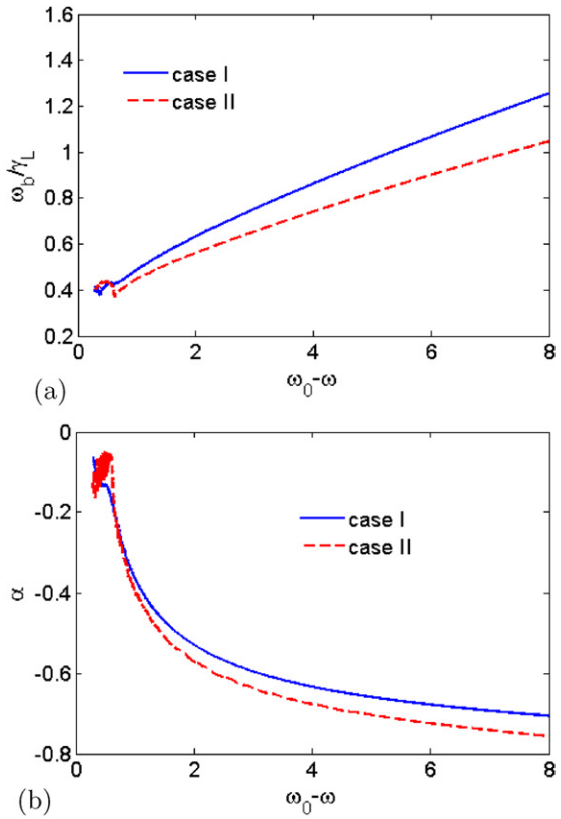


**Figure 1.** Comparison of the evolution of trapping frequency $\omega_b$ $(a)$ and chirping parameter $\alpha$ $(b)$ for two alternative damping cases in Vlasov simulations. The solid blue line depicts dissipation case (I) where the frequency is offset with an imaginary component $\gamma_d' = \gamma_d = 0.08$. The dashed line is for dissipation case (II) where the $\Delta_m$ parameter is offset with an imaginary component $\Delta_{i0} = -0.0623$.

To test the sensitivity to the dissipation mechanism, the results for a downshifting clump for the two alternative damping mechanisms, cases (I) and (II), are compared in figures 1$(a)$ and $(b)$ where a clump is tracked. The parameters chosen for the simulations in the figures are $\gamma_L = 0.1$ and $\Delta_r = 0.56$ with $\gamma_d = 0.08$ in case (I) and $\Delta_i = -0.0623$ in case (II). We see that there is the same general tendency for the two curves, but there are quantitative differences arising between the results of the two dissipation models. Similar results are found for an upshifting hole.

## 3. Adiabatic model

The particle–wave resonant structure can be derived from Hamilton–Jacobi theory. In systems where the Hamilton–Jacobi equation for the unperturbed orbits is separable, one can use the method, similar to the Schwarzschild transformation [11], to obtain action-angle variables to reduce the dimensions of a resonant system. For a sufficiently small perturbation, one can isolate a single resonance and select a transformation to the frame of the resonance structure, in the process of reducing the dynamics of the motion to a single action variable and its conjugate angle variable. One finds the following Hamiltonian

[5] for a frequency sweeping structure,

$$\mathcal{H} = \frac{P^2}{2} - \omega_b^2(\cos\theta - \alpha\theta). \tag{4}$$

Here, $P$ is the momentum of particles that are nearly resonant with the wave field, and $\theta$ is an action phase angle in the wave field. This Hamiltonian is a function of the wave amplitude $\omega_b^2$ and chirping parameter $\alpha \equiv \omega_b^{-2}\,\mathrm{d}\omega/\mathrm{d}t$, which leads to an asymmetric separatrix in $\theta$ about the O-point, where the energetic particles are deeply trapped. A normalized Hamiltonian-like form can be used to simplify the analysis to one parameter $\alpha$,

$$h = \frac{p^2}{2} - \cos\theta + \alpha\theta \tag{5}$$

where $p = P/\omega_b$, $h = \mathcal{H}/\omega_b^2$. When the parameters $\alpha$ and $\omega_b^2$ evolve slowly, the appropriate action $J$ is an adiabatic invariant and is given by

$$\begin{aligned} J = \frac{j\omega_b}{2\pi} &= \frac{1}{\pi}\int_{\theta_{\min}}^{\theta_{\max}} P\,\mathrm{d}\theta \\ &= \frac{\sqrt{2}\omega_b}{\pi}\int_{\theta_{\min}}^{\theta_{\max}} \sqrt{e(J)+\cos\theta-\alpha\theta}\,\mathrm{d}\theta. \end{aligned} \tag{6}$$

Here $e = h(p,\theta)$ is a normalized energy which for trapped particles takes on the range of values from $-\alpha\arcsin\alpha - \sqrt{1-\alpha^2}$ to $-|\alpha|\pi + \alpha\arcsin\alpha + \sqrt{1-\alpha^2}$ and $j$ is a normalized action variable. It is worth noting that $J$ is an adiabatic invariant but $j$ is not. The angles $\theta_{\max}$ and $\theta_{\min}$ are the points on the separatrix where the momentum $p$ vanishes. The positions of O and X points $\theta_{\mathrm{O}}$, $\theta_{\mathrm{X}}$, and range of $e$ are determined by the conditions

$$\begin{gathered} \frac{\partial h(p,\theta_{\mathrm{O,X}})}{\partial\theta} = 0 \\ \frac{\partial^2 h(p,\theta_{\mathrm{O}})}{\partial^2\theta} > 0; \quad \frac{\partial^2 h(p,\theta_{\mathrm{X}})}{\partial^2\theta} < 0 \\ h(p,\theta_{\mathrm{O}}) \leqslant e \leqslant h(p,\theta_{\mathrm{X}}). \end{gathered} \tag{7}$$

During the evolution, the action $J$ is assumed to be conserved from a time $t$ to $t+\Delta t$. Hence, $f(J)$ only changes due to the evolution of the separatrix value, $J_{\mathrm{spx}}(t)$. If $J_{\mathrm{spx}}$ increases, the new distribution at the separatrix becomes $f[J_{\mathrm{spx}}(t+\Delta t)] = F_0[\omega(t+\Delta t) \pm J_{\mathrm{spx}}(t+\Delta t)]$, with the + sign for $\omega > \omega_0$ and a minus sign for $\omega < \omega_0$, where $\omega_0$ is the frequency predicted from linear theory. For example, the newly created value of the trapped distribution function at $t = t_1$, $f(J_{\mathrm{spx}}, t = t_1)$ then remains constant in time (i.e. $f(J = J_{\mathrm{spx}}, t) = f(J_{\mathrm{spx}}, t = t_1)$) as long as the value of $J_{\mathrm{spx}}$ at a time $t > t_1$ satisfies $J_{\mathrm{spx}}(t) > J_{\mathrm{spx}}(t_1)$. This value $f(J_{\mathrm{spx}}, t_1)$ is stored and used for the subsequent evolution of the phase space structure. On the other hand, if $J_{\mathrm{spx}}$ decreases, the distribution at the separatrix changes with the new $f(J_{\mathrm{spx}})$ coming from a previously interior $J$-value in the trapped region whose $J$-value is equal to the new $J_{\mathrm{spx}}$.

The adiabatic response of the LHS of the wave equation, equation (1), is approximately the band filtered signal in the wave frame. The form for the RHS was derived in [3, 12]. The resulting adiabatic equations are given by

$$\begin{aligned} \Re(\Delta_m - \sqrt{\frac{1+\widetilde{\omega}}{1-\widetilde{\omega}}})\omega_b &= \frac{\eta}{\pi}\int_0^{\frac{J_{\mathrm{spx}}}{\omega_b}} \mathrm{d}j\,(f(\omega_b j) - F_0(\omega_b j)) \\ &\quad\times \int_0^{2\pi}\mathrm{d}\phi\cos\theta, \\ \Im(\Delta_m - \sqrt{\frac{1+\widetilde{\omega}}{1-\widetilde{\omega}}})\omega_b &= -\frac{\eta}{\pi}\int_0^{\frac{J_{\mathrm{spx}}}{\omega_b}} \mathrm{d}j\,(f(\omega_b j) - F_0(\omega_b j)) \\ &\quad\times \int_0^{2\pi}\mathrm{d}\phi\sin\theta \\ &= 2\alpha\eta\int_0^{\frac{J_{\mathrm{spx}}}{\omega_b}} \mathrm{d}j\,(f(\omega_b j) - F_0(\omega_b j)). \end{aligned} \tag{8}$$

$F_0(J)$ is the unperturbed distribution function normalized with the property that $(\mathrm{d}F_0(J)/\mathrm{d}J) = 1$, and $\widetilde{\omega} = \omega + \mathrm{i}\gamma_{\mathrm{d}}'$. The canonical angle $\phi$ for the perturbed system is determined from the relation

$$\mathrm{d}\phi = \frac{\pi\,\mathrm{d}\theta}{\sqrt{e(J)+\cos\theta-\alpha\theta}} \Big/ \int_{\theta_{\min}}^{\theta_{\max}} \frac{\mathrm{d}\theta}{\sqrt{e(J)+\cos\theta-\alpha\theta}}. \tag{9}$$

In the absence of dissipation and drive ($\eta = 0$), one finds (see [1, 5]) from the linear theory of equations (1) and (2) that the linear frequency $\omega_0$ is given by $\omega_0 = (\Delta_r^2 - 1)/(\Delta_r^2 + 1)$. When we take into account drive and dissipation under the assumption $\gamma_{\mathrm{L}} \ll 1$, we find a growth rate $\gamma$ given by $\gamma = \gamma_{\mathrm{L}} - \gamma_{\mathrm{d}}$, with $\gamma_{\mathrm{L}} = 4\pi\Delta_r\eta/(\Delta_r^2+1)^2 = \pi\eta/\lambda$, $\gamma_{\mathrm{d}} = \gamma_{\mathrm{d}}' - 4\Delta_r\Delta_{\mathrm{i}}/(\Delta_r^2+1)^2$. Case (I) discussed in the previous section has $\Delta_{\mathrm{i}} = 0$ so then $\gamma_{\mathrm{d}}' = \gamma_{\mathrm{d}}$, while case (II) has $\gamma_{\mathrm{d}}' = 0$, and then $\Delta_{\mathrm{i}} = -\gamma_{\mathrm{d}}(\Delta_r^2+1)^2/(4\Delta_r) = -\lambda\gamma_{\mathrm{d}} \equiv \Delta_{\mathrm{i}0}$. In general we have $\gamma_{\mathrm{d}}' = \beta\gamma_{\mathrm{d}}$ and $\Delta_{\mathrm{i}} = (1-\beta)\Delta_{\mathrm{i}0}$ with $0 \leqslant \beta \leqslant 1$. We also assume that the contribution of the untrapped particles to the perturbation is small, so that their contribution outside the separatrix is negligible and hence neglected.

To evaluate the angular integration in the RHS of the first term in equations (8), we consider the function $M$ and its derivative.

$$M(e) = 2\sqrt{2}\omega_b\int_{\theta_{\min}}^{\theta_{\max}} \sqrt{e(J)+\cos\theta-\alpha\theta}\cos\theta\,\mathrm{d}\theta, \tag{10}$$

$$\begin{aligned} \frac{\mathrm{d}M(J)}{\mathrm{d}J} &= \frac{\mathrm{d}M(J(e))/\mathrm{d}e}{\mathrm{d}J(e)/\mathrm{d}e} = \frac{2\pi\int_{\theta_{\min}}^{\theta_{\max}} \frac{\cos\theta\,\mathrm{d}\theta}{\sqrt{e(J)+\cos\theta-\alpha\theta}}}{\int_{\theta_{\min}}^{\theta_{\max}} \frac{\mathrm{d}\theta}{\sqrt{e(J)+\cos\theta-\alpha\theta}}} \\ &= \int_0^{2\pi}\cos\theta\,\mathrm{d}\phi. \end{aligned}$$

Then, the double integral can be written as

$$\Re(\Delta_m - \sqrt{\frac{1+\widetilde{\omega}}{1-\widetilde{\omega}}})\omega_b = \frac{\eta}{\pi}\int_0^{\frac{J_{\mathrm{spx}}}{\omega_b}} \mathrm{d}j\,(f(J) - F_0(J))\frac{\mathrm{d}M}{\mathrm{d}J}. \tag{11}$$

Here, the functions $M$ and $J$ are calculated near the separatrix on a fine grid of $e(J)$ and the derivative $\mathrm{d}M/\mathrm{d}J$ is constructed with high accuracy in use of a cubic spline. A trapezoidal rule is used in the $J$ integration from 0 to $J_{\mathrm{spx}}$.

During the evolution of the system, the time scale for change is much longer than a wave period, while the time step in the Vlasov simulation has to be smaller than the wave period. Therefore, if the adiabatic assumption for the phase space structure is fulfilled, the adiabatic equations enable more

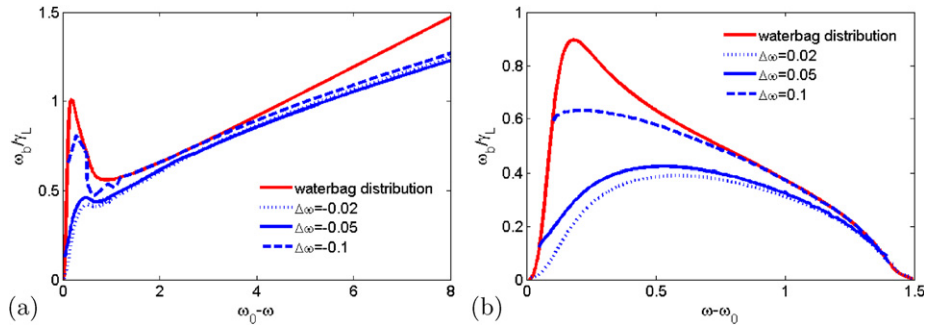


**Figure 2.** Adiabatic prediction (for dissipation case (I)) for amplitude evolution of a clump (*a*) and hole (*b*). $\gamma_L = 0.1$, $\gamma_d = 0.08$, $\Delta_m = 0.654$ and $\eta = 0.0248$. The blue curves are for self-consistent adiabatic responses that evolve from an initial waterbag distribution displaced from linear frequency by various $\Delta\omega$ values. The red curve is for a distribution constrained to be a waterbag with a discontinuity at the trapped particle separatrix.

rapid predictions of the wave evolution than one would obtain from the direct Vlasov simulation. However, the accuracy of the adiabatic equations is ensured only if the response remains adiabatic during the evolution.

In the simulation, the adiabatic approximation is never formally justified at the birth of a resonant structure as the quantities $\omega_b$ and $\alpha$ initially change very rapidly. Nonetheless, we initiate our problem early in the formation process, where the adiabatic approximation is not valid and we find, as will be shown below, that the subsequent adiabatic evolution is close to numerical simulation results. To begin with, a small resonant waterbag structure is assumed present centred at an initial frequency $\omega_0 + \Delta\omega$ slightly shifted from the linear frequency $\omega_0$. This waterbag distribution is constant for all particles trapped inside the separatrix region, given by $F_0$ for all $J$ values less than the separatrix value $J = J_{spx}$, while the distribution just outside separatrix discontinuously changes to $F_0 = \omega_0 + J_{spx}$. The two relations in equations (8) are then solved for $\omega_b$ and $\alpha$. We find that a solution to equations (8) can be obtained even for a small value of the deviation $\Delta\omega$ from the linear frequency, such as $\Delta\omega \sim 0.2\gamma_L$. Having found an initial solution, we scan the frequency $\omega$ and solve for $\omega_b(\omega)$ and $\alpha(\omega)$. The time dependence of the solution can also be found by integrating, $\omega_b^{-2}\,\mathrm{d}\omega/\mathrm{d}t = \alpha$.

The numerical results, arising from the choice of case (I), are shown in figure 2(*a*) for the clump and figure 2(*b*) for the hole. These solutions show that the TAE waves, initially excited in the gap $-1 \leqslant \omega \leqslant 1$, chirp as clumps move towards the lower continuum ($\omega = -1$) and as holes move towards the upper continuum ($\omega = 1$). The clump shown in figure 2(*a*) penetrates the lower tip and then evolves with an increasing wave amplitude. The sensitivity of the response to the initial frequency displacement $\Delta\omega$ has been investigated. There is sensitivity in the early response to $\Delta\omega$. We will see in the next section that the best fit, of the adiabatic theory with the simulation, results when $\Delta\omega \sim 0.5\gamma_L$.

Figures 2(*a*) and (*b*) also show the results predicted from treating the distribution function as a waterbag, whose discontinuity is at the separatrix of the trapped particles. One then finds the following equations determining the evolution,

$$\Re(\Delta_m - \sqrt{\frac{1+\widetilde{\omega}}{1-\widetilde{\omega}}})\omega_b = \frac{\lambda\gamma_L}{\pi^2}(1-\alpha^2)^{7/4}d_1(\alpha)\Delta f(J)$$
$$\Im(\Delta_m - \sqrt{\frac{1+\widetilde{\omega}}{1-\widetilde{\omega}}})\omega_b = \frac{\lambda\gamma_L}{\pi^2}\alpha(1-\alpha^2)^{5/4}d_2(\alpha)\Delta f(J) \quad (12)$$

where the functions $d_1(\alpha)$ and $d_2(\alpha)$ are smooth monotonic and slowly varying functions of $\alpha$, given by,

$$d_1(\alpha) = 2\sqrt{2}(1-\alpha^2)^{-7/4} \times \int_{\theta_{min}}^{\theta_{max}} \mathrm{d}\theta\sqrt{(1-\alpha^2)^{1/2} - |\alpha|\pi + \alpha\arcsin\alpha + \cos\theta - \alpha\theta} \times \cos\theta = 16c_1(\alpha), \quad (13)$$
$$d_2(\alpha) = 2\sqrt{2}(1-\alpha^2)^{-5/4} \times \int_{\theta_{min}}^{\theta_{max}} \mathrm{d}\theta\sqrt{(1-\alpha^2)^{1/2} - |\alpha|\pi + \alpha\arcsin\alpha + \cos\theta - \alpha\theta} = 16c_2(\alpha),$$

whose values, as the magnitude of $\alpha$ goes from 0 to 1, vary from $\frac{1}{3}$ to $\frac{3}{14}$ for $c_1(\alpha)$ and from 1 to $\frac{3}{10}$ for $c_2(\alpha)$ along the separatrix determined from the normalized Hamiltonian equation (5). We also note that there is error in [12] for values of $c_1$ and $c_2$ as $|\alpha|$ approaches unity, and in particular $c_1$ does not change sign in contrast to [12] as $|\alpha|$ goes from 0 to 1.

In obtaining equation (12) we have assumed that the distribution remains a waterbag with $f(J)$ constant in the trapping region at the value $F_0(J) = \omega_0$ where $\omega_0$ is the $J$ value of the unperturbed particles at the original linear frequency. Just outside the separatrix $f = F_0(\omega \pm J_{spx})$, so there is a discontinuity $\Delta f(J) = \omega \pm J_{spx} - \omega_0$ at the separatrix. The assumption of a discontinuous waterbag distribution at the separatrix is maintained, even when the bounding separatrix increases during the evolution. In contrast the consistently evaluated distribution is continuous as $J_{spx}$ increases. Nonetheless we see that there is general qualitative agreement of the mode amplitude and chirping parameter with the consistent theory but with a significant quantitative difference, particularly early in the evolution.

## 4. Comparison of adiabatic theory with kinetic model

The adiabatic model is derived from our basic equations assuming that the adiabatic approximation is valid during the entire evolution of the phase space structure. Agreement of the predictions of the adiabatic and simulation results implies that the adiabatic model captures the essential dynamics being produced in the simulation.

First we compare the theoretical adiabatic response of a down-chirping clump to the results found in the simulation.

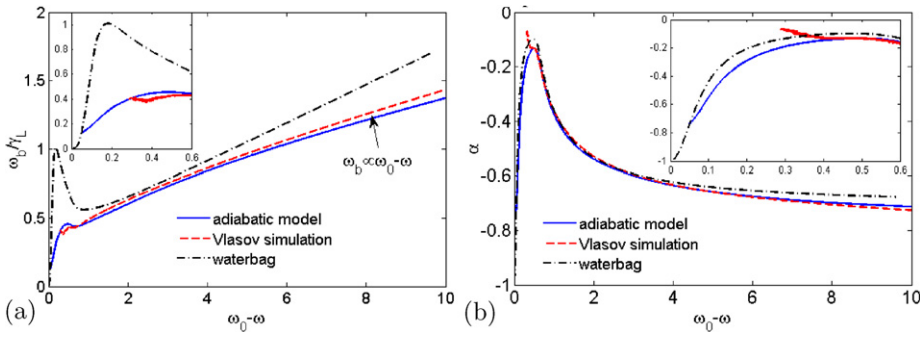


**Figure 3.** Comparison, using case (I), for a clump between the predications of adiabatic theory and simulation results, for the mode amplitude, $\omega_b$ $(a)$ and chirping parameter $\alpha$ $(b)$. Comparison of the results for the crude waterbag model is also shown. System parameters are $\Delta_m = 0.654$, $\eta = 0.0248$, $\gamma_L = 0.1$, $\gamma_d = 0.08$, $\Delta\omega = 0.5\gamma_L$. The inserted figures resolve the response when the frequency is in the gap $(0 \leqslant \omega_0 - \omega \leqslant 0.6)$.

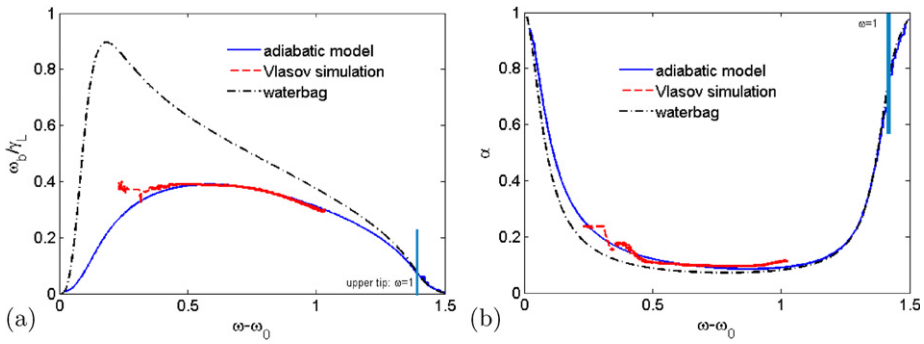


**Figure 4.** Comparison of predictions for $\omega_b$ $(a)$ and $\alpha$ $(b)$ between the Vlasov simulation and adiabatic model for an evolving hole structure for dissipative case (I). Same input parameters as figure 3.

The initial adiabatic solution is obtained by assuming an initial waterbag distribution at the bounding separatrix present with a frequency, $\Delta\omega$, shifted slightly from the linear mode frequency. One can then solve the adiabatic equations given by equations (8) for $\omega_b(\omega)$ and $\alpha(\omega)$. A comparison for a clump of $\omega_b(\omega)$ and $\alpha(\omega)$ between what is predicted by the adiabatic theory and simulations are shown for dissipative case (I) in figures 3$(a)$ and $(b)$. Similar good comparisons, not shown here, have been obtained for dissipative case (II) as well.

We find very good results for a hole in the mid-range of $\omega - \omega_0$, as is seen in figures 4$(a)$ and $(b)$ which are the results for the dissipative case (I), where $\gamma_d' = \gamma_d$. However, for early times when the frequency shift is very small we do not extract reliable data from the simulation because the noise is high (higher than that for a clump with the same magnitude of frequency shift). Thus, for the simulation in figures 4$(a)$ and $(b)$, we only show the filtered results of $\omega_b(\omega)$ and $\alpha(\omega)$ when $\omega - \omega_0$ is larger than 0.25, when the filtering of the noise becomes manageable. In the frequency range $0.25 \leqslant \omega - \omega_0 \leqslant 1.05$ there is excellent correlation between the adiabatic theory's predicted values for $\omega_b(\omega)$ and $\alpha(\omega)$ compared with the values produced in the simulation. However, the hole appears to disintegrate when $\omega - \omega_0 > 1.05$.

Thus we conclude, for the down-chirping clump and the up-chirping hole, that the agreement between the Vlasov simulation and the consistent adiabatic model is impressively good for both cases, as long as the chirping structure stays intact in the simulation. The reason for the hole's disintegration is not firmly established. However, a candidate explanation for the loss of the hole is the breakdown of the adiabaticity assumption as the hole approaches the upper continuum. In figures 5$(a)$ and $(b)$ we show an adiabaticity breakdown parameter, $P_{adb}$, where a smaller $P_{adb}$ means better reliability of the adiabatic prediction (the definition of $P_{adb}$ is discussed at the end of this section). We see in the figure on the left that the breakdown parameter suddenly begins to rise at $\omega - \omega_0 \sim 1.2$, a number close to where the hole disintegrates in the simulation. We still need to confirm whether the deterioration of adiabaticity leads to the loss of the hole. Another candidate reason is the onset of as yet an unidentified instability, or simply the accumulation of numerical error. We also note that case (II) does not exhibit sudden deterioration, just a slow decay in amplitude as the frequency approaches the upper continuum. For this case, the adiabatic theory is consistent even for small amplitude, because the adiabatic parameter, $P_{adb}$, remains small.

There are several other points worth noting. In the early stages of evolution, it is seen in figure 5 that an initial small hole does not satisfy the adiabaticity condition as the parameters change very rapidly. The trapping frequency at the O-point, $\Omega_b$, is given by $\Omega_b = \omega_b(1-\alpha^2)^{1/4}$. The simplest criterion to fulfil the adiabaticity condition for particles at the O-point is

$$\frac{1}{\Omega_b^2}\frac{d\Omega_b}{dt} \ll 1. \tag{14}$$

Since $d/dt = \omega_b^2 \alpha d/d\omega$, this criterion is equivalent to

$$\left|\alpha(1-\alpha^2)^{-5/4}\left[(1-\alpha^2)\frac{d\omega_b}{d\omega} - \frac{1}{2}\omega_b\alpha\frac{d\alpha}{d\omega}\right]\right| \ll 1 \tag{15}$$

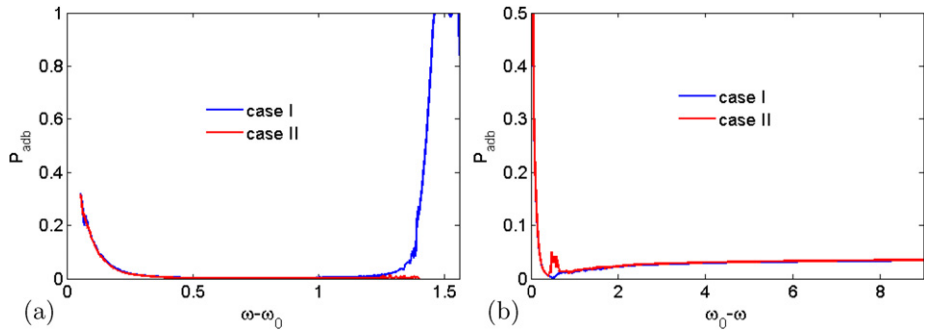


**Figure 5.** Study of evolution of the adiabaticity parameter as a function of frequency shift for both hole ($a$) and clump ($b$) for the two extreme dissipative cases (I) and (II).

We see that if $\alpha^2$ is close to unity it is likely that the adiabaticity criterion will fail. Nonetheless the comparison of the results from the adiabatic and simulation runs, from the creation of a phase space structure to its late evolution, is generally excellent. What appears to be important for an accurate prediction of the evolution is that the distribution fills in smoothly, as it does both in the actual simulation and in the case of an initially small waterbag core where the separatrix surrounding the trapped particles grows during the chirp.

In addition the adiabatic approximation is suspect when a clump goes through the tip point at $\omega = -1$. In this case the local adiabatic approximation for model (II) cannot be justified due to an abrupt change of the parameters of the adiabatic equations in equations (8). We see in figure 5($b$) that adiabatic parameter $P_{\rm adb}$ decreases markedly as the frequency chirps towards $\omega = -1$, where $\omega_0 - \omega \approx 0.6$. However, close to $\omega = -1$, the adiabatic parameter suddenly begins to increase quite markedly for case (II) ($\gamma_{\rm d}' = 0$) and only modestly for case (I) ($\gamma_{\rm d}' = \gamma_{\rm d}$). However, $P_{\rm adb}$, still remains small, even for case (I). Hence, the disturbance producing an adiabaticity violation remains moderate, and the resulting comparisons of adiabatic theory with the simulation remain accurate even as the chirping structure goes through the continuum boundary as well as deep into the continuum.

A more restrictive adiabatic condition is based on the following considerations. First we note as the parameters, $\omega_b$ and $\alpha$ vary slowly in time, that a particle's action along its actual trajectory varies during a bounce time and it is only the mean value, which we have denoted as $J$, that remains constant during the evolution of the particle's motion. There is then a maximum variation of the action $\delta J(J)$ from the mean value $J$ during a single bounce of the particle. We have analytically evaluated $\delta J(J)$ by standard means. Then if $\delta J(J)$ is larger than the difference between the separatrix $J_{\rm spx}$ and $J$, i.e. $J_{\rm spx} - J$, this particle has a high probability of being untrapped, which is a violation in the assumption of the constancy of $J$. We then solve for that action, $J_{\rm cr}$ that satisfies the condition $\delta J(J_{\rm cr}) = J_{\rm spx} - J_{\rm cr}$ which enables us to define $P_{\rm adb}$ as $P_{\rm adb} \equiv \delta J(J_{\rm cr})/J_{\rm spx}$. Then as a criterion for the validity of adiabaticity for most of the particles trapped in the phase space structure, we require $P_{\rm adb} \ll 1$.

The adiabaticity parameter, $P_{\rm adb}$, for the hole and clump runs given in figures 5($a$) and ($b$) shows very small numbers for $P_{\rm adb}$ except for the initial states when $|\alpha|$ is somewhat less than unity and near the upper continuum for the hole in case (II). Hence the adiabatic model gives excellent results compared with the Vlasov simulation except for a hole near the upper continuum.

## 5. Analysis of adiabatic theory

The relatively complicated structure of equations (8) makes them difficult to solve analytically over the entire domain of the chirp especially as it is difficult to analytically calculate the correct distribution function $f(J)$ when the separatrix is rising. We can simplify the problem by assuming that the distribution in the trapping region is always a waterbag distribution described in the previous section. We will use this waterbag assumption to study properties of the chirping mode for a clump structure at the lower continuum frequency and its later chirp when it is deep into the Alfvén continuum a great deal below the lower tip frequency. We also study the adiabatic chirping properties of a hole should the frequency get close to the upper tip.

The waterbag model from equations (12) predicts the bounce frequency (i.e. square root of wave amplitude) and chirping parameter at the lower tip, is given by

$$\frac{\omega_b}{\gamma_{\rm L}} = \frac{\lambda(1+\omega_0)\Delta_r^{5/2} d_1(\alpha) d_2(\alpha)^{7/2}}{\pi^2((\Delta_{\rm i} d_1(\alpha))^2 + (\Delta_r d_2(\alpha))^2)^{7/4}} = 0.62,$$
$$\alpha = \frac{\Delta_{\rm i} d_1(\alpha)}{((\Delta_{\rm i} d_1(\alpha))^2 + (\Delta_r d_2(\alpha))^2)^{1/2}} = -0.132 \qquad (16)$$

where the numerical values are calculated using the parameters given in the caption of figure 3. As can be seen in figure 3($a$), this predicted chirping parameter is quite similar to the simulation result, while $\omega_b/\gamma_{\rm L}$ is a factor ~1.5 larger than the prediction of the consistent model. Also note in figure 3($b$), that the waterbag model prediction is significantly different from the consistent adiabatic results when the frequency is in the gap but much closer for frequencies in the continuum.

Deep in the continuum ($\omega_0 - \omega \gg 1$), the chirping parameter $\alpha$, plotted in figure 3($b$) approaches a constant value and the bounce frequency in figure 3($a$) grows linearly with $\omega$. This behaviour is apparent from a local analysis of the equations for the waterbag model, equations (12), under the

assumption $\omega \gg 1$, where one finds

$$\omega_b \Delta_r = \frac{\lambda \gamma_L}{\pi^2}(1-\alpha^2)^{7/4} d_1(\alpha)(\omega_0 - \omega),$$
$$\omega_b = \frac{\lambda \gamma_L}{\pi^2}\alpha(1-\alpha^2)^{5/4} d_2(\alpha)(\omega_0 - \omega). \tag{17}$$

Dividing these two equations, we obtain an implicit function of $\alpha$. A simplified expression is obtained if we use the value $\alpha^2 = 1$ in $d_1$ and $d_2$. Then we find that deep in the continuum,

$$\alpha \to \alpha_{-\infty} \doteq -\frac{1}{\sqrt{1.96\Delta_r^2 + 1}} = -0.74. \tag{18}$$

This value appears to be within 10% of the value found in the simulation as seen in figure 1(*b*). Such a solution leads to an explosive growth in the time domain as follows from the evolution equation,

$$\alpha = \omega_b^{-2}\frac{\mathrm{d}\omega}{\mathrm{d}t} = \omega_b^{-2}\frac{\mathrm{d}\omega_b}{\mathrm{d}t}\frac{\mathrm{d}\omega}{\mathrm{d}\omega_b} = \frac{\pi^2 \omega_b^{-2}}{\lambda\gamma_L \alpha(1-\alpha^2)^{5/4} d_2(\alpha)}\frac{\mathrm{d}\omega_b}{\mathrm{d}t}. \tag{19}$$

This equation, solved for $\alpha = \alpha_{-\infty}$, has an explosive response, which is proportional to $(t_\infty - t)^{-1}$. The undetermined constants can be obtained by curve fitting to the numerical solutions of the adiabatic waterbag equations.

$$\omega_b(t) = \frac{\omega_{b0} t_\infty}{t_\infty - t} \qquad (t_\infty = 6448, \omega_{b0} = 0.0322). \tag{20}$$

A similar procedure can be used to study the behaviour of the adiabatic response of a hole near the upper continuum. Simulations indicate that the hole disappears before the frequency gets too close to the continuum and thus the adiabatic theory for this case cannot be compared with simulation results. We present the detailed analysis of how a hole approaches the upper continuum in the appendix. The analysis demonstrates that for dissipative case (II), where the dissipation $\Delta_i$ is finite and $\gamma_d' = 0$, the chirping mode does not penetrate the continuum. As the continuum is approached $\alpha$ becomes small and $\omega_b$ vanishes in proportion to $\sqrt{1-\omega}$. However, when $\gamma_d'$ is nonzero, the hole slightly penetrates into the continuum, and then decays to zero amplitude when $\omega = 1 + (\gamma_d'/\sqrt{2}\Delta_r)^{2/3}$.

## 6. Summary

Frequency chirping frequently arises after the spontaneous excitation of waves in a plasma when there is a close balance of the drive from the free energy source present to amplify the waves together with a nearly matching sink of dissipation which causes wave damping in the absence of a free energy source. The chirp is due to the formation of clump and/or hole structures as a result of wave trapping of resonant particles. Then, as an alternative to the amplitude damping, the energy released by the free energy source is absorbed by the dissipative sink while the phase space structures move to a lower energy state. This movement of the trapping structure in phase space produces the observed chirping signal which is locked to the phase space positions of the holes and clumps [12].

The constancy of the trapped particle action in a slowly evolving wave enables an adiabatic description of the system in terms of a relatively simple set of equations based on a Hamiltonian that explicitly includes the chirping term but implicitly includes the time. Most other studies of this problem have assumed either $\alpha \ll 1$ or $\alpha \approx 1$. Whenever the adiabatic theory is justified we can avoid a more expensive simulation of studying chirps, based on solving the Vlasov equation by a direct numerical integration. Indeed we find that our reduced adiabatic description usually gives impressive agreement with direct numerical simulation results. When we find a disparity of the adiabatic theory prediction with numerical observations, as occurred when holes attempt to reach the upper continuum, we find that the adiabatic solutions lead to an increase in value of the adiabaticity parameter, $P_{adb}$, which indicates that the adiabaticity theory could be failing. On the other hand, early in the simulation, we find that even though there is a large adiabaticity parameter that would lead one to distrust the validity of the early calculation when the phase structures are small, the best results of the simulation are achieved when very small initial seeds for holes or clumps are taken. Perhaps a reason for this is that a small initial seed leads to a relatively smooth trapped distribution around the separatrix, rather than a waterbag distribution, with an abrupt transition at the separatrix. In the simulation one would expect that the intrinsic non-adiabatic behaviour near the separatrix would cause a smooth distribution to develop. The development of a similar smooth distribution in the adiabatic calculation may then give a more accurate prediction during the later evolution when the adiabaticity assumption is justified because a more realistic distribution, than that from a waterbag, has formed.

Our study may have application to the observations of strong sweeping events in MAST [13]. It is possible that the results of this simulation, which indicate that downward chirp originating in the gap is capable of sweeping through a large frequency range while upward frequency chirp has a limited range of sweeping, captures the fundamental mechanism that governs the experimental data. Here, and in the experiment, there is preferential frequency sweeping into the lower continuum where then there is further enhancement of the chirping signal as it moves through the continuum. Perhaps this pattern captures an essential physics feature that is responsible for the experimental data. However, the basic physics of our modelling of the energetic particles and wave interaction must still be improved before the mechanism of the wave penetration into the continuum can be considered valid. In addition our model is for large aspect ratio tokamak, while MAST is a small aspect ratio tokamak. Nonetheless, the mechanisms we are uncovering may well be independent of the aspect ratio.

As an example of missing physics that may be essential to the theory is that the interaction term of the particle Hamiltonian may depend on the wave frequency and particle momentum, as is the case for the Hamiltonian derived in [14] for the RBV model. Inclusion of these effects, which is now under investigation, will add essential realism to the calculation and then a more reliable assessment can be made as to whether the hole-clump chirping theory gives an accurate physical model for interpreting experimental data.

## Appendix A. Adiabatic theory for hole near the upper continuum

Using the waterbag model while examining frequencies close to the upper continuum where $|1-\omega| \ll 1$ and $\gamma_d \ll 1$, the two adiabatic equations can be written approximately as

$$\omega_b\left(\Delta_r - \Re\left(\frac{2}{1-\widetilde{\omega}}\right)^{1/2}\right) = -\frac{\lambda\gamma_L}{\pi^2}(1-\alpha^2)^{7/4}d_1(\alpha)(1-\omega_0),$$
$$\omega_b\left(\Delta_i - \Im\left(\frac{2}{1-\widetilde{\omega}}\right)^{1/2}\right) = -\frac{\lambda\gamma_L}{\pi^2}\alpha(1-\alpha^2)^{5/4}d_2(\alpha)(1-\omega_0), \tag{A.1}$$

with $d_1$ and $d_2$ given in equations (13). We also introduce a parameter $\beta$ defined as $\beta = \gamma_d'/\gamma_d$, and then $\Delta_i = (1-\beta)\Delta_{i0}$, where $\Delta_{i0} = -\lambda\gamma_d$, with $\lambda = (\Delta_r^2+1)^2/(4\Delta_r)$, which produces the same damping rate $\gamma_d$, for all values of $\beta$. Then equation (A.1) can be written as

$$\omega_b\left[\Delta_r - \sqrt{\frac{\sqrt{(1-\omega)^2+(\beta\gamma_d)^2}+1-\omega}{(1-\omega)^2+(\beta\gamma_d)^2}}\right] = -\frac{\lambda\Delta_r}{\pi^2}\gamma_L(1-\alpha^2)^{7/4}d_1(\alpha)(1-\omega_0), \tag{A.2}$$
$$\omega_b\left[(1-\beta)\Delta_{i0} - \sqrt{\frac{\sqrt{(1-\omega)^2+(\beta\gamma_d)^2}-1+\omega}{(1-\omega)^2+(\beta\gamma_d)^2}}\right] = -\frac{\lambda\gamma_L}{\pi^2}\alpha(1-\alpha^2)^{5/4}d_2(\alpha)(1-\omega_0).$$

Dividing the two equations with each other to eliminate $\omega_b$, we obtain

$$\frac{\sqrt{\sqrt{(1-\omega)^2+(\beta\gamma_d)^2}-(1-\omega)} - \Delta_{i0}(1-\beta)\sqrt{(1-\omega)^2+(\beta\gamma_d)^2}}{\sqrt{\sqrt{(1-\omega)^2+(\beta\gamma_d)^2}+(1-\omega)} - \Delta_r\sqrt{(1-\omega)^2+(\beta\gamma_d)^2}} = \frac{\alpha d_2(\alpha)}{(1-\alpha^2)^{1/2}d_1(\alpha)}. \tag{A.3}$$

As the upper continuum is approached from below, we first consider the region where $\beta\gamma_d \ll (1-\omega) \ll 1$. Then we find that in this region $\alpha \ll 1$ and is approximately given by

$$\alpha = \frac{1}{3\sqrt{2}}(1-\omega)^{1/2}\left(-\Delta_{i0}(1-\beta) + \frac{\beta\gamma_d}{\sqrt{2}(1-\omega)^{3/2}}\right). \tag{A.4}$$

For the dissipative case (II), where $\beta = 0$, we see that $\alpha$ goes monotonically to zero as $\omega$ approaches unity. Then from equations (A.1), we find that $\omega_b = \lambda\gamma_L/3\sqrt{2}\pi^2(1-\omega_0)\sqrt{1-\omega}$.

If $\beta \neq 0$ it can also be shown that $\alpha$ continues to decrease as $\omega$ approaches unity as long as the inequality $1-\omega \gg \beta\gamma_d$ continues to be valid. However, when this inequality is invalid, $1-\omega \sim \beta\gamma_d$ a rather complicated function of $1-\omega$ results where the solution for $\alpha$ increases to a value that is an order-unity fraction less than 1. In addition $\omega$ always penetrates the continuum for non-zero $\beta$. At $\omega = 1$, we find in the limit of $\gamma_d \ll \max(1, 1/\Delta_r^2)$, $\alpha$ satisfies,

$$\frac{\alpha d_2(\alpha)}{(1-\alpha^2)^{1/2}d_1(\alpha)} = 1, \tag{A.5}$$

with the solution $\alpha = 0.645$ independent of the value of $\beta$, while the bounce frequency is,

$$\omega_b = 0.69\beta^{1/2}\lambda\gamma_L\gamma_d^{1/2}(1-\omega_0). \tag{A.6}$$

After penetration into the continuum, $\alpha$ increases and heads towards unity. When $\beta\gamma_d \ll \omega - 1 \sim (\beta\gamma_d)^{2/3}$, $\alpha^2$ is given by

$$\alpha^2 = 1 - 1.96\left(\frac{\beta\gamma_d}{2(\omega-1)} - \frac{\Delta_r}{\sqrt{2}}(\omega-1)^{1/2}\right)^2. \tag{A.7}$$

The maximum frequency, $\omega_{mx}$, is found to be

$$\omega_{mx} = 1 + \left(\frac{\beta\gamma_d}{\sqrt{2}\Delta_r}\right)^{2/3}. \tag{A.8}$$

In this region $\omega - 1 \sim (\beta\gamma_d)^{2/3}$, $\omega_b$ goes to zero as

$$\omega_b = 0.05\lambda\gamma_L(1-\omega_0)\sqrt{\omega-1} \times \left(\frac{\beta\gamma_d}{2(\omega-1)} - \frac{\Delta_r}{\sqrt{2}}(\omega-1)^{1/2}\right)^{5/2}. \tag{A.9}$$

## References


[1] Cheng C.Z. and Chance M.S. 1986 Low-*n* shear Alfvén spectra in axisymmetric toroidal plasmas *Phys. Fluids* **29** 3695–701

[2] O'Neil T.M., Winfrey J.H. and Malmberg J.H. 1971 Nonlinear interaction of a small cold beam and a plasma *Phys. Fluids* **14** 1204–12

[3] Berk H.L., Breizman B.N. and Petviashvili N.V. 1997 Spontaneous hole-clump pair creation in weakly unstable plasmas *Phys. Lett.* A **234** 213–8

[4] Lilley M.K., Breizman B.N. and Sharapov S.E. 2009 Destabilizing effect of dynamical friction on fast-particle-driven waves in a near-threshold nonlinear regime *Phys. Rev. Lett.* **102** 195003

[5] Wang G. and Berk H.L. 2012 Model for spontaneous frequency sweeping of an Alfvén wave in a toroidal plasma *Commun. Nonlinear Sci. Numer. Simul.* **17** 2179–90

[6] Rosenbluth M.N., Berk H.L., van Dam J.W. and Lindberg D.M. 1992 Mode structure and continuum damping of high-*n* toroidal Alfvén eigenmodes *Phys. Fluids* B **4** 2189–202

[7] Nyqvist R.M., Lilley M.K. and Breizman B.N. 2012 Adiabatic description of long range frequency sweeping *Nucl. Fusion* **52** 094020

[8] Petviashvili N.V. 1998 Coherent structures in nonlinear plasma dynamics *PhD Dissertation* University of Texas at Austin, Department of Physics

[9] Gottlieb D. and Shu C.-W. 1997 On the Gibbs phenomenon and its resolution *SIAM Rev.* **39** 644–68

[10] Shannon C.E. 1949 Communication in the presence of noise *Proc. IRE* **37** 10–21

[11] Ferraz-Mello S. (ed) 2007 *Canonical Perturbation Theories—Degenerate Systems and Resonance* (*Astrophysics and Space Science Library* vol 345) (New York: Springer)

[12] Berk H.L., Breizman B.N., Candy J., Pekker M. and Petviashvili N.V. 1999 Spontaneous hole-clump pair creation *Phys. Plasmas* **6** 3102–13

[13] Gryaznevich M.P. and Sharapov S.E. 2006 Perturbative and non-perturbative modes in START and MAST *Nucl. Fusion* **46** S942

[14] Berk H.L., Breizman B.N. and Ye H. 1993 Map model for nonlinear alpha particle interaction with toroidal Alfvén waves *Phys. Fluids* B **5** 1506–15